J. Fluid Mech. (2008), *vol.* 605, *pp.* 181–206.
doi:10.1017/S002211200800147X Printed in the United Kingdom

Mathematical modelling of non-axisymmetric capillary tube drawing

I. M. GRIFFITHS AND P. D. HOWELL

Mathematical Institute, 24–29 St Giles', Oxford, OX1 3LB, UK

(Received 10 August 2007 and in revised form 10 March 2008)

This paper concerns the manufacture of non-axisymmetric capillary tubing via the Vello process, in which molten glass is fed through a die and drawn off vertically. The shape of the cross-section evolves under surface tension as it flows downstream. The aim is to achieve a given desired final shape, typically square or rectangular, and our goal is to determine the required die shape.

We use the result that, provided the tube is slowly varying in the axial direction, each cross-section evolves like a two-dimensional Stokes flow when expressed in suitably scaled Lagrangian coordinates. This allows us to use a previously derived model for the surface-tension-driven evolution of a thin two-dimensional viscous tube. We thus obtain, and solve analytically, equations governing the axial velocity, thickness and circumference of the tube, as well as its shape. The model is extended to include non-isothermal effects.

1. Introduction

This study is motivated by the industrial manufacture of glass capillary tubing with a specified cross-sectional shape. In particular, an interest has developed in the production of tubing with a square or rectangular cross-section. The tubes may be used, for example, to make medicine bottles (Pfaender 1996) or square cross-sectional optical fibres (Wu, Somervell & Barnes 1998; Wu *et al.* 2000). As illustrated in figure 1, molten glass is fed through a die and the glass tubing is drawn off vertically, before being cut to rough length by a cutter. The rate of flow of glass through the die is controlled by varying its temperature and hence viscosity. The profile of the cross-section varies downstream of the die in response to surface tension, and additional control may be achieved by applying an internal pressure (Uhlmann & Kreidl 1984). Our ultimate aim is to solve the inverse problem of determining the die shape required to achieve a given final (e.g. square) cross-section.

The drawing of non-axisymmetric simply connected fibres has been considered by, for example, Denn (1980), Dewynne, Ockendon & Wilmott (1989) and Cummings & Howell (1999). In Cummings & Howell (1999), for fibre drawing with slow variations in the axial direction, the shape of the cross-section was found to satisfy a two-dimensional time-dependent Stokes flow problem when expressed in suitable scaled Lagrangian coordinates. The drawing of hollow optical fibres has also been studied previously, for example by Fitt *et al.* (2001), who concentrate on axisymmetric fibres, so the shape of the cross-section is uniformly circular. Here the main concern is evolution in the size of the hole, and the large aspect ratio of the fibre is exploited to obtain quasi-one-dimensional models. The extension to multiple-holed tubing is important in the drawing of micro-structured optical fibres, and is addressed by Voyce, Fitt & Monro (2004).

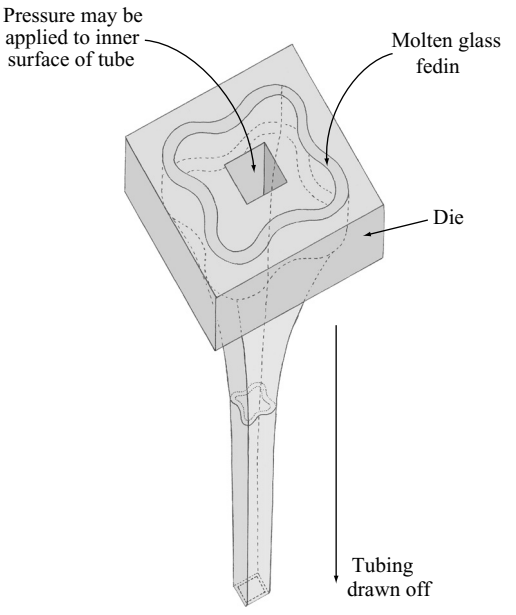

FIGURE 1. Schematic diagram of the Vello process for the construction of square capillary tubing.

Production of non-isothermal simply connected tubing has also been studied in detail (see, for example, Lee & Jaluria 1997; Papamichael & Miaoulis 1991; Paek & Runk 1978). However while bearing certain similarities to capillary tube manufacture, this considers only axisymmetric fibres, which are manufactured by drawing out a preform, with particular emphasis on the manufacture of tubing for optical fibres. This is extended to cover hollow tubing by Fitt *et al.* (2002), motivated by the practical applications of hollow optical fibres.

In this paper we are concerned with the production of tubing that is both non-axisymmetric and hollow. To make the problem more tractable we make two simplifying assumptions. First we suppose that the tube varies slowly in the axial direction. This allows us to reduce the problem to a quasi-one-dimensional system of partial differential equations governing the axial flow coupled to a two-dimensional biharmonic problem for the crossflow, as in Cummings & Howell (1999). Our second assumption is that the tube wall is thin compared with its circumference, so we can exploit the theory developed by Griffiths & Howell (2007) for a thin-walled two-dimensional annular domain of viscous fluid, or *viscida* (Buckmaster, Nachman & Ting 1975; Buckmaster & Nachman 1978). By combining these ideas we obtain a quasi-one-dimensional model that describes the axial velocity, the cross-sectional area and circumference and a reduced time that parameterizes the evolution of the cross-section shape.

We begin by considering the simplified constant-viscosity case to demonstrate the *modus operandi*. We state the full governing equations and boundary conditions in § 2 before non-dimensionalizing and taking the appropriate asymptotic limits in §3. We omit the details of the asymptotic analysis, quoting the relevant leading-order equations from Cummings & Howell (1999) and Griffiths & Howell (2007). The zero-Reynolds-number limit is considered in § 4. The explicit solution of the resulting equations is used to determine the regions of parameter-space where a viable, stable

Parameter	Symbol	Approx. value	Units
Surface tension	γ	0.3	$\mathrm{N\,m^{-1}}$
Density	ρ	2500	$\mathrm{kg\,m^{-3}}$
Viscosity	μ	10^3–10^8	$\mathrm{N\,s\,m^{-2}}$
Tubing length	D	1.5	m
Final circumference	L_d	0.05	m
Final thickness	h_d	1	mm
Input speed	w_0	10^{-3}	$\mathrm{m\,s^{-1}}$
Draw ratio	R	10–30	—

TABLE 1. Typical parameter values for the drawing of capillary glass tubing (Graham 1987; U. Lange, personal communication 2006; Šarboh *et al.* 1998; Sivko 1976).

tube can be formed, and some typical solutions are presented. In § 5, we then generalize the problem to include non-isothermal effects, following a similar solution procedure.

2. Governing equations and boundary conditions

2.1. *Geometry of the tubing*

We consider tubing lying between a die at $z = 0$ and a final position $z = D$ where it is cut off, with a cross-sectional profile that we wish to specify. We concentrate in this paper on the steady draw-down of tubing with uniform thickness in each cross-section. Hence the tubing thickness h and the cross-sectional centreline circumference L are functions only of z; generalizations to unsteady flows may be found in Griffiths (2008).

In table 1 we show typical parameter values for the tube-drawing problem. Figure 2 shows a schematic diagram of the set-up. We assume that the tubing is both long and thin, implemented specifically by defining the two parameters ϵ and δ,

$$\epsilon = \frac{h_d}{L_d} \ll 1, \qquad \delta = \frac{L_d}{D} \ll 1, \tag{2.1}$$

where $L_d = L(D)$ and $h_d = h(D)$ are respectively the centreline circumference and thickness of the tubing at the final section $z = D$. The typical parameter values in table 1 give $\epsilon \approx 0.02$ and $\delta \approx 0.033$.

Note that ϵ and δ are defined in terms of the final tube profile, this geometry being a known requirement of the problem. Since our goal is to determine the initial die profile, defining ϵ and δ in terms of the geometry at the die would result in these parameters having to be found as part of the solution, thus complicating the analysis. However, for consistency, one should check *a posteriori* that the corresponding values of ϵ and δ at the die are small.

2.2. *Governing equations and boundary conditions*

We shall begin by considering the surface-tension-driven evolution of a tube with constant viscosity and negligible gravity. The fluid flow in the tubing is governed by the steady Navier–Stokes equations

$$\nabla \cdot \boldsymbol{u} = 0, \tag{2.2}$$

$$\rho\,(\boldsymbol{u} \cdot \nabla)\,\boldsymbol{u} = -\nabla p + \mu \nabla^2 \boldsymbol{u}, \tag{2.3}$$

where $\boldsymbol{u} = u\boldsymbol{i} + v\boldsymbol{j} + w\boldsymbol{k}$ and p denote the fluid velocity and pressure.

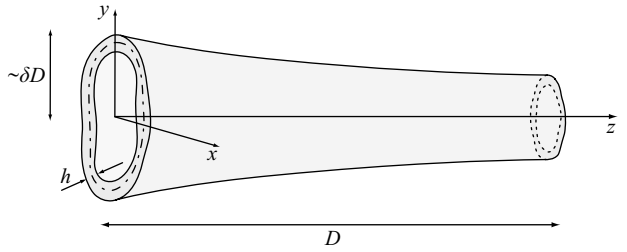

FIGURE 2. Definition sketch of a slender thin viscous tubing. The dot-dash line represents the centreline of a section through the tube at a given axial position z.

If we define the positions of the inner (−) and outer (+) surfaces of the tube by the level sets $G^{\pm}(x, y, z) = 0$, then we may write the kinematic and dynamic boundary conditions on the inner and outer surfaces of the tubing respectively as

$$\boldsymbol{u} \cdot \nabla G^{\pm} = 0, \tag{2.4a}$$

$$\boldsymbol{\sigma} \cdot \nabla G^{\pm} = \mp \gamma \kappa^{\pm} \nabla G^{\pm}, \tag{2.4b}$$

on $G^{\pm} = 0$, where $\kappa^{\pm}$ are the mean curvatures of the outer and inner surfaces respectively, and $\boldsymbol{\sigma} = \{\sigma_{ij}\}$ is the usual Newtonian stress tensor, given by

$$\sigma_{ij} = -p\delta_{ij} + \mu \left(\frac{\partial u_i}{\partial x_j} + \frac{\partial u_j}{\partial x_i} \right). \tag{2.5}$$

The problem is closed by specifying the velocity at the two ends of the tubing, say

$$\boldsymbol{u} = \boldsymbol{u}_1 \quad \text{at} \quad z = 0, \qquad \boldsymbol{u} = \boldsymbol{u}_2 \quad \text{at} \quad z = D, \tag{2.6}$$

as well as the shape of the cross-section at either $z = 0$ or $z = D$. In the forward problem, the shape of the die at $z = 0$ is given; however, we are concerned with the inverse problem in which the desired shape at $z = D$ is prescribed and the corresponding die shape is to be determined. Hence we suppose that $G^{\pm}(x, y, D)$ are given functions.

3. Perturbative analysis

3.1. *Non-dimensionalization*

We now non-dimensionalize the system to exploit the two small parameters, ϵ and δ:

$$(x, y, z) = D(\delta x', \delta y', z'), \qquad h = \epsilon \delta D h', \qquad L = \delta D L', \tag{3.1a}$$

$$u = (u, v, w) = w_0(\delta u', \delta v', w'), \qquad p = \frac{\mu w_0}{D} p', \qquad \kappa^{\pm} = \frac{1}{\delta D} \kappa^{\pm\prime}. \tag{3.1b}$$

Henceforth we drop the primes on dimensionless variables. We begin by performing a systematic perturbative analysis with respect to δ, expanding all dependent variables as regular parameter expansions of the form $u' = u^{(0)} + \delta^2 u^{(1)} + \cdots$, and similarly for all other dependent variables. We omit the details of this procedure, which closely follow that given in Cummings & Howell (1999, §§2, 3). The resulting leading-order equations are then simplified further by exploiting the smallness of ϵ.

3.2. *The axial flow equations*

For simply connected fibres, the leading-order flow is extensional, so the leading-order axial velocity $w^{(0)} = w^{(0)}(z)$ is uniform over each cross-section. With superscripts dropped, the leading-order equations governing the axial flow are (Cummings & Howell 1999)

$$\frac{\mathrm{d}}{\mathrm{d}z}(w\mathscr{S}) = 0, \tag{3.2}$$

$$Re\mathscr{S}w\frac{\mathrm{d}w}{\mathrm{d}z} = \frac{\mathrm{d}}{\mathrm{d}z}\left(3\mathscr{S}\frac{\mathrm{d}w}{\mathrm{d}z}\right) + \frac{1}{2\delta Ca}\frac{\mathrm{d}\Gamma}{\mathrm{d}z}, \tag{3.3}$$

where $\mathscr{S}$ and Γ are the leading-order area and circumference of the cross-section respectively. The Reynolds and capillary numbers are defined by

$$Re = \frac{\rho w_0 D}{\mu}, \quad Ca = \frac{\mu w_0}{\gamma}. \tag{3.4}$$

It is a simple exercise to extend the derivation given by Cummings & Howell (1999 § 3 and Appendix A and B) and hence show that (3.2) and (3.3) apply also to a hollow tube (see Griffiths 2008, Chapter 5). In this case, the leading-order cross-sectional area of the tube is $\mathscr{S} = \mathscr{S}^+ - \mathscr{S}^-$, where $\mathscr{S}^\pm$ are the cross-sectional areas bounded by the outer and inner interfaces, while Γ is simply identified with the net circumference $\Gamma^+ + \Gamma^-$ of the cross-section.

Now, under the additional assumption that the tube wall is thin, we can approximate $\mathscr{S}$ and Γ by

$$\frac{\mathscr{S}}{\epsilon} = S \sim hL, \quad \Gamma \sim 2L, \tag{3.5}$$

recalling that $h(z,t)$ and $L(z,t)$ are the dimensionless wall thickness and perimeter of the centre-surface. Hence (3.2) and (3.3) become

$$\frac{\mathrm{d}}{\mathrm{d}z}(wS) = 0, \tag{3.6}$$

$$RewS\frac{\mathrm{d}w}{\mathrm{d}z} = \frac{\mathrm{d}}{\mathrm{d}z}\left(3S\frac{\mathrm{d}w}{\mathrm{d}z}\right) + \gamma^*\frac{\mathrm{d}L}{\mathrm{d}z}, \tag{3.7}$$

where the relevant dimensionless surface-tension coefficient is

$$\gamma^* = \frac{1}{\epsilon\delta Ca} = \frac{\gamma D}{\mu w_0 h_d}. \tag{3.8}$$

3.3. *The crossflow problem*

So far we have the two axial flow equations (3.6) and (3.7) in the three unknowns S, L and w. To make further progress, we must now consider the crossflow in the (x, y)-plane. For a simply connected fibre, Cummings & Howell (1999) showed that this flow is equivalent to a two-dimensional surface-tension-driven Stokes flow when expressed in suitable scaled Lagrangian variables. Again, it is a straightforward exercise to extend their analysis to describe an annular cross-section, and the details are presented in Griffiths (2008, Appendix D). Since the crossflow problem is non-mass-conserving due to axial stretching we first define cross-sectional variables

$$x^* = \frac{x}{\sqrt{S}}, \quad y^* = \frac{y}{\sqrt{S}}, \tag{3.9}$$

scaled so that the area of each cross-section is constant (and equal to ϵ) with respect to (x^*, y^*). Next we define the Lagrangian time variable $\tau(z)$ in the axial direction satisfying

$$w\frac{\mathrm{d}\tau}{\mathrm{d}z} = \frac{\gamma^*}{\sqrt{S}}, \qquad \tau(1) = 0. \tag{3.10}$$

Note that τ is initialized at the downstream end where the final tube shape is to be specified.

Any material cross-section, propagating axially at speed $w(z)$, evolves like a classical planar Stokes flow, with surface-tension coefficient equal to ϵ, with respect to the new variables, x^*, y^* and τ. This two-dimensional problem has been analysed in the limit of small wall thickness by Griffiths & Howell (2007), who show that the circumference and thickness of the cross-section satisfy

$$L^* = \frac{1}{1+\tau/2}, \qquad h^* = 1 + \frac{\tau}{2} \tag{3.11}$$

(Griffiths & Howell 2007, equations (3.17) and (3.18)). Notice that our choice of non-dimensionalization implies that $S = L = h = 1$ at $z = 1$, which corresponds to $\tau = 0$. The circumference and thickness with respect to unscaled coordinates are hence given by

$$L = \frac{\sqrt{S}}{1+\tau/2}, \qquad h = \sqrt{S}\left(1 + \frac{\tau}{2}\right). \tag{3.12}$$

Equation (3.12) may be used to substitute for τ in (3.10) to obtain

$$w\frac{\mathrm{d}}{\mathrm{d}z}\left(\frac{S}{L^2}\right) = \frac{\gamma^*}{L}. \tag{3.13}$$

This equation and the axial mass and momentum balances (3.6) and (3.7) give us a closed system of ordinary differential equations for S, w and L. We will present solutions of this problem below in § 4, but first we show how to determine the shape of the tubing.

3.4. *Evolution of the cross-section shape*

It is interesting that the problem derived above depends on the shape of the cross-section only through its area S and circumference L. The detailed dynamics of the cross-section shape therefore decouples from that of S, w and L. Since each scaled material cross-section satisfies a canonical two-dimensional Stokes flow problem for the evolution of an annular domain, its evolution is in principle determined completely, as a function of τ, by its initial shape. To map this back to physical variables we just have to (i) rescale by a factor of $\sqrt{S}$ and (ii) relate τ back to z using (3.10).

For thin-walled tubing, with spatially uniform thickness given by (3.12), to determine the shape of the tubing at each axial cross-section we need only determine the position of the centreline of the cross-section. As shown in Griffiths & Howell (2007, §§ 2, 3), this is most readily achieved using angle/arclength coordinates that are scaled with the circumference L^*, that is,

$$x^* = \frac{X(\xi,\tau)}{1+\tau/2}, \qquad y^* = \frac{Y(\xi,\tau)}{1+\tau/2}, \tag{3.14}$$

where

$$\frac{\partial X}{\partial \xi} = \cos\theta, \qquad \frac{\partial Y}{\partial \xi} = \sin\theta. \tag{3.15}$$

Here, $\theta(\xi, \tau)$ denotes the angle made with the centreline of the cross-section, and $0 \leqslant \xi \leqslant 1$ represents the arclength around the centreline in this coordinate system which is scaled with the circumference.

The shape of the cross-section is thus determined parametrically by the function $\theta(\xi, \tau)$, which is shown to satisfy the partial differential equation

$$\frac{\partial}{\partial \tau}\left[(1+\tau/2)\frac{\partial^2 \theta}{\partial \xi^2}\right] = A(\tau)\sin\theta + B(\tau)\cos\theta \tag{3.16}$$

(equation (3.21), Griffiths & Howell 2007). The arbitrary functions A and B are determined as part of the solution from the boundary conditions

$$\theta(0,\tau) = 0, \quad \theta(1,\tau) = 2\pi, \quad \int_0^1 \cos\theta \, \mathrm{d}\xi = \int_0^1 \sin\theta \, \mathrm{d}\xi = 0. \tag{3.17a–c}$$

Condition (3.17*c*) ensures that the ends are joined, while (3.17*a*) fixes the orientation of the profile, eliminating the arbitrary rigid body rotation, and (3.17*b*) ensures that the join is smooth.

The initial condition for (3.16) is specification of the final tubing shape $\theta(\xi, 0) = \theta_0(\xi)$. Then we wish to solve (3.16) in $\tau < 0$ to determine the cross-sectional profile as we move up the tubing toward the die. As discussed in Griffiths & Howell (2007, § 4) this problem is, surprisingly, well posed for inverse time. Indeed, for profiles with rotational symmetry, A and B are identically zero so that (3.16) admits the exact analytic solution

$$\theta(\xi,\tau) = \frac{\theta_0(\xi) - 2\pi\xi}{1+\tau/2} + 2\pi\xi. \tag{3.18}$$

For profiles with no rotational symmetry, (3.16) is readily soluble numerically.

In this paper, we will focus on the final shape given by

$$\theta_0(\xi) = \begin{cases} 0, & 0 < \xi < 1/8 - \pi/4k, \\ k(\xi - 1/8) + \pi/4, & 1/8 - \pi/4k < \xi < 1/8, \end{cases} \tag{3.19}$$

and the symmetry conditions

$$\theta_0\left(\frac{1}{4} \pm \xi\right) \equiv \frac{\pi}{2} \pm \theta_0(\xi). \tag{3.20}$$

As shown in figure 3(*a*), this represents a square with rounded corners. The parameter $k \in (2\pi, \infty)$ measures the rounding, with the profile approaching a circle as $k \to 2\pi$ and a square as $k \to \infty$. With $\theta(\xi, \tau)$ given by (3.18), it is straightforward to integrate (3.15) analytically and hence obtain

$$X = \begin{cases} \dfrac{2+\tau}{2\pi\tau}\sin\left(\dfrac{2\pi\tau\xi}{2+\tau}\right), & 0 < \xi < \dfrac{1}{8} - \dfrac{\pi}{4k}, \\ \dfrac{2+\tau}{2\pi\tau(k+\pi\tau)}\left\{k\sin\left(\dfrac{(k-2\pi)\pi\tau}{4k(2+\tau)}\right)\right. & \\ \qquad \left. - \pi\tau\sin\left(\dfrac{k-2\pi-8(k+\pi\tau)\xi}{4(2+\tau)}\right)\right\}, & \dfrac{1}{8} - \dfrac{\pi}{4k} < \xi < \dfrac{1}{8}, \end{cases} \tag{3.21}$$

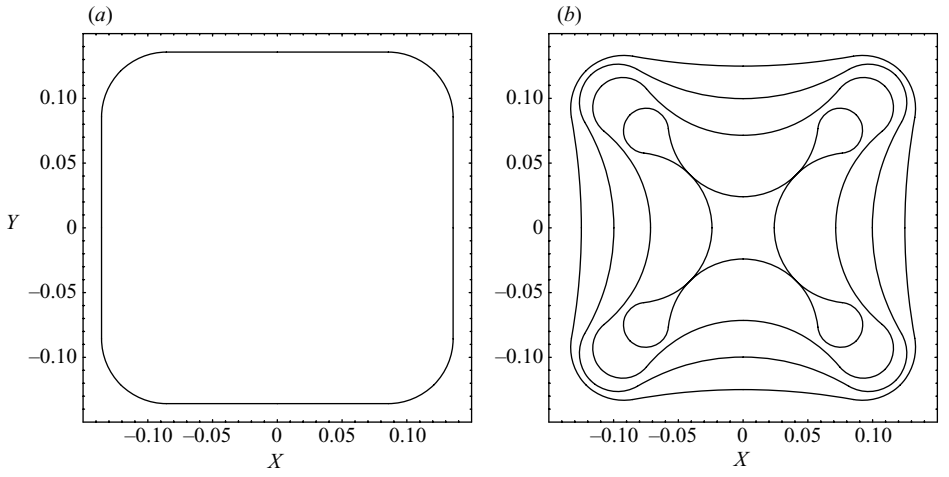

FIGURE 3. (*a*) The initial condition (3.19) with $k = 20$. (*b*) The evolution of the profile shown in (*a*) at times $\tau = -0.5, -1.0, -1.25, -1.46572$.

$$Y = \begin{cases} -\dfrac{2+\tau}{2\pi\tau}\cos\left(\dfrac{2\pi\tau\xi}{2+\tau}\right) \\ \quad + \dfrac{k(2+\tau)}{\sqrt{2}\pi\tau(k+\pi\tau)}\sin\left(\dfrac{\pi(k+\pi\tau)}{2k(2+\tau)}\right), \quad 0 < \xi < \dfrac{1}{8} - \dfrac{\pi}{4k}, \\ -\dfrac{2+\tau}{2\pi\tau(k+\pi\tau)}\left\{k\sin\left(\dfrac{(k-2\pi)\pi\tau}{4k(2+\tau)}\right)\right. \\ \quad \left. + \pi\tau\cos\left(\dfrac{k-2\pi-8(k+\pi\tau)\xi}{4(2+\tau)}\right)\right\}, \quad \dfrac{1}{8} - \dfrac{\pi}{4k} < \xi < \dfrac{1}{8}, \end{cases} \tag{3.22}$$

and the behaviour for all other values of ξ follows by symmetry. As shown in figure 3(*b*), the profile buckles inwards for negative values of τ, pinching off at a critical time $\tau_c \approx -1.46572$ when $k = 20$. The pinch-off time is an increasing function of k, with $\tau_c \to -2$ as $k \to 2\pi$ and $\tau_c \to -1$ as $k \to \infty$.

3.5. *Axisymmetric tubing*

Before presenting solutions, we now briefly show how our governing equations simplify when the cross-section is circular, for comparison with previous models of axisymmetric tube drawing. If the final cross-sectional centreline is circular then $\theta_0(\xi) = 2\pi\xi$, and (3.18) implies that $\theta(\xi, \tau) \equiv 2\pi\xi$ so, as expected, the profile remains circular throughout the tube. In this case, the cross-section area, thickness and circumference are related to the inner and outer radii, r_- and r_+ respectively, by

$$\epsilon S = \pi(r_+^2 - r_-^2), \quad \epsilon h = r_+ - r_-, \quad L = \pi(r_+ + r_-). \tag{3.23}$$

Hence the axial flow equations (3.6) and (3.7) take the form

$$\frac{\mathrm{d}}{\mathrm{d}z}(w(r_+^2 - r_-^2)) = 0, \tag{3.24}$$

$$Re\, w(r_+^2 - r_-^2)\frac{\mathrm{d}w}{\mathrm{d}z} = \frac{\mathrm{d}}{\mathrm{d}z}\left(3(r_+^2 - r_-^2)\frac{\mathrm{d}w}{\mathrm{d}z}\right) + \epsilon\gamma^*\frac{\mathrm{d}}{\mathrm{d}z}(r_+ + r_-). \tag{3.25}$$

Next, from the governing equation (3.13) for L, we deduce that $r_\pm$ satisfy

$$w\frac{\mathrm{d}}{\mathrm{d}z}\left(\frac{r_+^2-r_-^2}{(r_++r_-)^2}\right)=\frac{\epsilon\gamma^*}{r_++r_-}, \tag{3.26}$$

and use of (3.24) then leads to the equations

$$\frac{\mathrm{d}}{\mathrm{d}z}(wr_+^2)=\frac{\mathrm{d}}{\mathrm{d}z}(wr_-^2)=-\frac{\epsilon\gamma^*r_+r_-}{r_+-r_-}. \tag{3.27}$$

Equations (3.24), (3.25) and (3.27) for r_+, r_- and w are identical to those given in Fitt *et al.* (2002), confirming that our model for S, w and L is mathematically equivalent to the axisymmetric model.

4. The slow-flow limit

4.1. *Leading-order solution*

We have seen in § 3.2 and § 3.3 that inertia is important only in the axial flow problem. The typical parameter values in table 1 give $\gamma^*\sim 10^{-3}$–10^{2} and $Re\sim 10^{-8}$–10^{-3}, and we therefore concentrate henceforth on the slow-flow limit $Re\to 0$, while retaining γ^*. We impose the boundary conditions

$$w(0)=1,\quad w(1)=R,\quad S(1)=1,\quad L(1)=1, \tag{4.1a–d}$$

which follow from our choice of non-dimensionalization and define the draw ratio R, an important control parameter.

With $Re=0$, we may integrate (3.6) and (3.7) to give

$$wS=R, \tag{4.2}$$

$$3S\frac{\mathrm{d}w}{\mathrm{d}z}=6bR-\gamma^*L, \tag{4.3}$$

where b is a constant of integration; physically, $6b$ represents the net dimensionless tension applied to the tube. Equation (4.2) allows S to be eliminated from the problem so that (3.13) and (4.3) may be written as two first-order ordinary differential equations for L and w, namely

$$\frac{\mathrm{d}w}{\mathrm{d}z}=\frac{(6bR-\gamma^*L)\,w}{3R}, \tag{4.4}$$

$$\frac{\mathrm{d}L}{\mathrm{d}z}=-\frac{(3bR+\gamma^*L)\,L}{3R}. \tag{4.5}$$

These are readily solved, subject to the boundary conditions (3.1b,d), to give

$$w=\frac{3bR^2\mathrm{e}^{-2b(1-z)}}{\gamma^*+3bR-\gamma^*\mathrm{e}^{b(1-z)}}, \tag{4.6}$$

$$S=\frac{\mathrm{e}^{2b(1-z)}}{3bR}\left(\gamma^*+3bR-\gamma^*\mathrm{e}^{b(1-z)}\right), \tag{4.7}$$

$$L=\frac{3bR\mathrm{e}^{b(1-z)}}{\gamma^*+3bR-\gamma^*\mathrm{e}^{b(1-z)}}. \tag{4.8}$$

We can then infer the tube wall thickness h from (3.5) and the Lagrangian time variable τ from (3.12):

$$h(z)=\frac{S(z)}{L(z)},\qquad \tau(z)=2\left(\frac{\sqrt{S(z)}}{L(z)}-1\right). \tag{4.9}$$

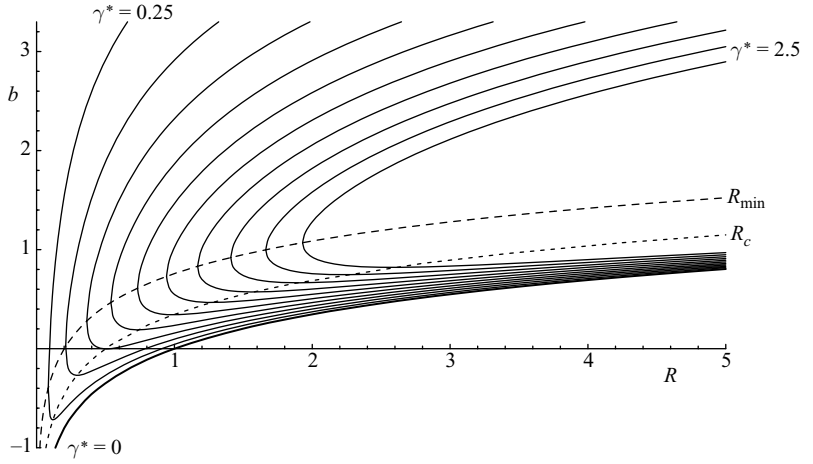

FIGURE 4. Scaled tension b versus draw ratio R for values of the surface tension parameter $\gamma^* = 0, 0.25, 0.5 \ldots, 2.5$. The minimum and critical draw ratios, $R_{\min}$ and R_c are shown as dashed lines.

The centreline of each cross-section is thus given parametrically by

$$\begin{pmatrix} x \\ y \end{pmatrix} = L(z) \begin{pmatrix} X(\xi, \tau(z)) \\ Y(\xi, \tau(z)) \end{pmatrix}, \tag{4.10}$$

with $(X(\xi, \tau), Y(\xi, \tau))$ given by (3.21).

4.2. *Parametric analysis*

It remains to determine the constant b from the boundary condition (3.1a), which leads to the equation

$$R^2 - \mathrm{e}^{2b} R + \gamma^* \mathrm{e}^{2b} \frac{\mathrm{e}^b - 1}{3b} = 0. \tag{4.11}$$

For a given γ^*, we can thus use (4.11) to obtain the scaled tension b as a function of the draw ratio R. The resulting behaviour of b versus R is shown in figure 4 for various values of γ^*.

As $\gamma^* \to 0$, the solution of (4.11) reduces to

$$b = \tfrac{1}{2} \ln R \quad \text{when } \gamma^* = 0. \tag{4.12}$$

For each positive value of γ^*, we observe that there is a minimum draw ratio $R_{\min}(\gamma^*)$ below which no steady solution exists. When R exceeds $R_{\min}$, there are two possible values of b corresponding to each R, and hence two possible solutions of the boundary-value problem. We illustrate their typical behaviour in figure 5, where we show w, S, L and h as functions of z when $\gamma^* = 2$ and $R = 2$. In this case the two possible values of b are $b \approx 0.66801$ and $b \approx 1.82053$. We observe that the larger value of b gives physically implausible behaviour, with the velocity w initially decreasing sharply near the die before increasing to its given value of 2 at $z = 1$. Furthermore, the circumference L grows alarmingly near $z = 0$ (to approximately 117.736 which is off the scale of the graph), while the thickness becomes close to zero. It seems unlikely that such solutions could be stable, and we infer that we should choose the lower branch of the (R, b) curves shown in figure 4. Indeed, it is this lower branch that converges to the zero-surface-tension limit (4.12) as $\gamma^* \to 0$.

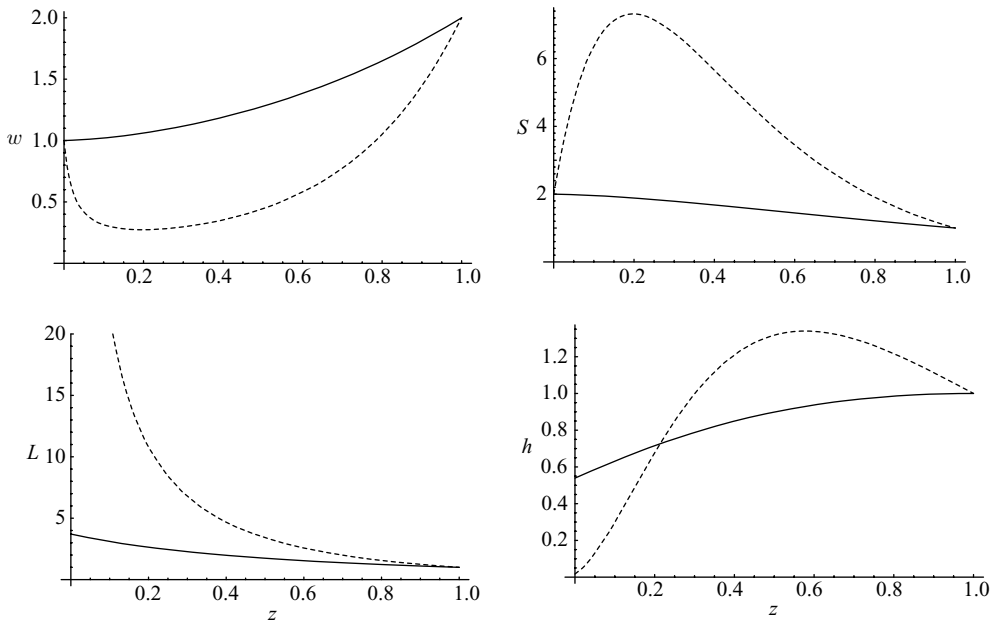

FIGURE 5. Axial velocity w, cross-section area S, tube circumference L and thickness h versus axial position z with $\gamma^* = 2$, $R = 2$ and $b = 0.66801$ (solid), $b = 1.82053$ (dashed).

By choosing the lower of the two available values of b, we can now obtain a unique solution for any given γ^* and R, provided $R > R_{\min}(\gamma^*)$. However, it is equally possible in practice to control the tension applied to the tube, in which case the draw ratio is determined by the problem. Since the lower branch of figure 4 is non-monotonic, we may still face non-uniqueness in such problems where b is specified rather than R. In figure 4, we show as a dotted line the critical value $R = R_c(\gamma^*)$ corresponding to the minimum value of b. For $R_{\min} < R < R_c$, we see that the tension is a decreasing function of the draw speed, and this configuration surely cannot be stable. (Such instabilities are considered in Wylie, Huang & Miura 2007.) We therefore hypothesize that the lower branch is stable only when $R > R_c(\gamma^*)$, in which case we have a well-defined invertible mapping between R and b.

To limit further the range of possible solutions, we note that when $\gamma^* < 3/4$ there is a range of values of R for which b is negative. We would expect a positive tension to be required to extrude the fluid from the die. Moreover, a negative tension would probably lead to a sinuous instability in the tube (Howell 1996), and we therefore exclude solutions with $b < 0$.

We show the (γ^*, R) parameter-space in figure 6. The minimum draw ratio $R_{\min}(\gamma^*)$, given parametrically by

$$R_{\min} = \mathrm{e}^{2b}\frac{(b-1)\mathrm{e}^b + 1}{(3b-1)\mathrm{e}^b + 1 - 2b}, \quad \gamma^* = 6b^2\mathrm{e}^{2b}\frac{(b-1)\mathrm{e}^b + 1}{((3b-1)\mathrm{e}^b + 1 - 2b)^2}, \tag{4.13}$$

is plotted as a dotted curve. The critical value $R_c(\gamma^*)$, corresponding to the minimum value of b, satisfies the implicit equation

$$\gamma^* = \frac{3R_c \ln(2R_c)}{4\left(\sqrt{2R_c} - 1\right)} \tag{4.14}$$

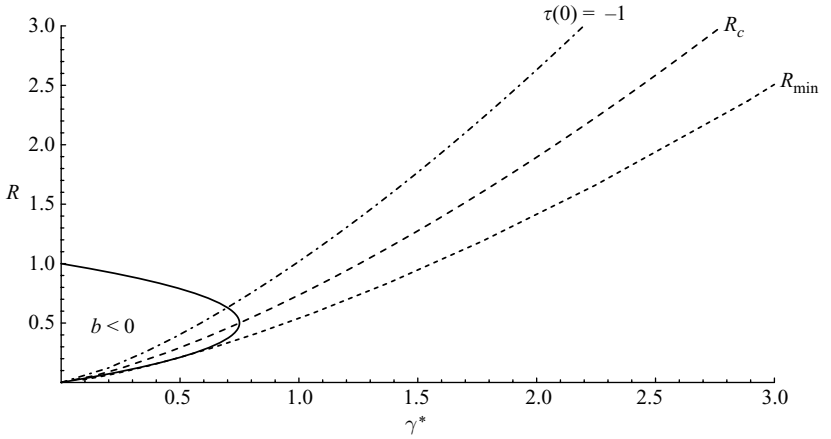

FIGURE 6. Parameter-space of draw ratio R versus surface tension parameter γ^*. The dotted line shows the minimum draw ratio $R_{\min}(\gamma^*)$. The dashed line shows the critical value $R_c(\gamma^*)$ at which the tension b is minimized. The dot-dashed curve shows where the Lagrangian time variable τ is equal to -1 at $z = 0$. The solid curve delineates the region where b is negative.

and is shown as a dashed curve. Finally, the region leading to negative values of b is bounded by the solid curve

$$\gamma^* = 3R(1 - R). \tag{4.15}$$

This intersects the curve $R = R_c(\gamma^*)$ at $\gamma^* = 3/4$, $R = 1/2$ and is tangent to $R = R_{\min}(\gamma^*)$ at $\gamma^* = 12/25$, $R = 1/5$.

We have argued that physically meaningful and stable solutions can exist only where $R > R_c(\gamma^*)$ and $b > 0$. The parameter-space may be further restricted by the requirement that the tube does not pinch off. As illustrated in figure 3(b), there is a finite critical value of $\tau = \tau_c \in (-2, 0)$ at which the tube cross-section self-intersects, and, to avoid this, we must insist that $\tau(0) > \tau_c$. The curve in the (γ^*, R)-plane on which $\tau(0) = \tau_c$ is given by

$$\gamma^* = \frac{3R\left(1 - (1 + \tau_c/2)^{2/3}\right)}{2\left(\sqrt{R}(1 + \tau_c/2)^{-1/3} - 1\right)} \ln\left(\frac{R}{(1 + \tau_c/2)^{2/3}}\right), \tag{4.16}$$

which is identical to (4.14) when $\tau_c = 1/\sqrt{2} - 2 \approx -1.29289$. Hence our previously imposed condition $R > R_c(\gamma^*)$ ensures in addition that $\tau(0) > 1/\sqrt{2} - 2$. This is sufficient for the shape given in figure 3(a), for which $\tau_c \approx -1.46572$, but (4.16) leads to a stronger condition for larger values of τ_c. For example, if $\tau_c = -1$, then R must lie above the dot-dashed curve shown in figure 6.

4.3. *Typical solutions*

In summary, for slow flow we have found explicit analytical solutions for the extrusion of a slowly varying thin-walled tube. Figure 6 indicates the values of the draw ratio and the dimensionless surface tension for which a viable tube can be established. Within this parameter domain, the problem admits a unique solution, and we are able to predict explicitly the die shape corresponding to any given final tube cross-section. In figure 7, we show the three-dimensional profile leading to the final shape shown in figure 3 with $R = 2$, $\gamma^* = 2$. These parameter values are purely illustrative, and this solution corresponds to the solid curves in figure 5. The right-hand side of the

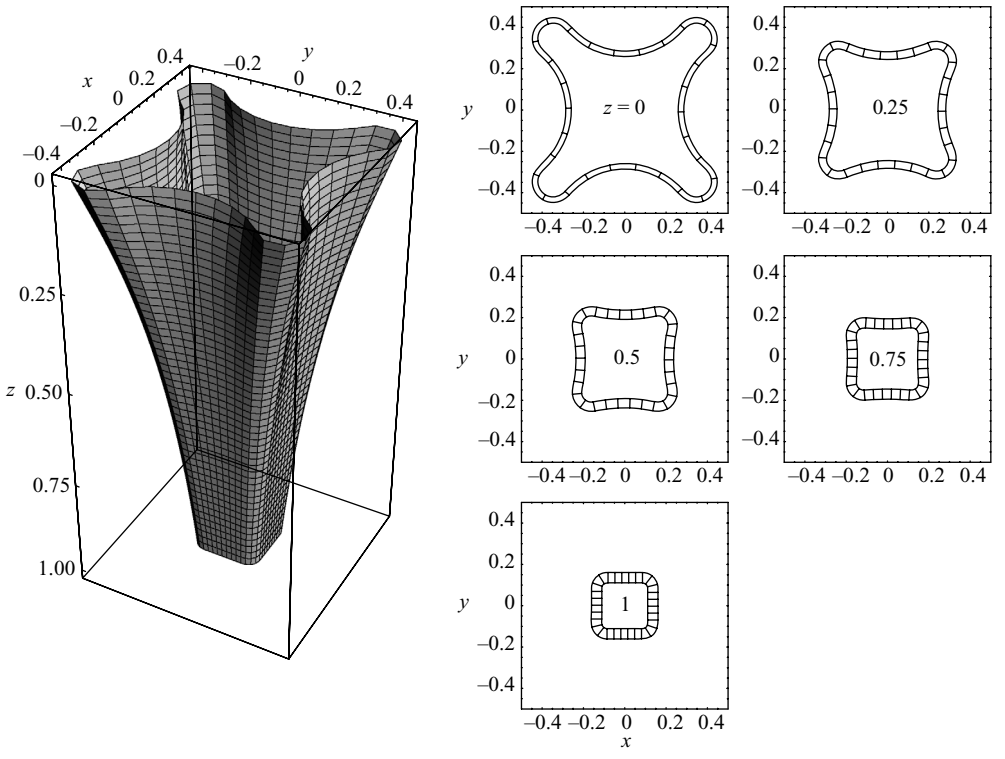

FIGURE 7. Three-dimensional centreline profile with $\gamma^* = 2$, $R = 2$ and $k = 20$, as well as cross-sections through the tube with $\epsilon = 0.05$.

figure shows the die shape required to achieve the desired final shape and how the cross-section evolves along the tube.

In figure 8, we show further illustrative solutions, with $\gamma^* = 2$ and increasing values of R. The velocity and area behave monotonically as expected, but the circumference is surprisingly insensitive to variations in the draw ratio. With a low draw ratio $R = 2$, the thickness increases as surface tension causes the tube to contract and thicken. On the other hand, the largest draw ratio $R = 5$ causes the tube to thin monotonically due to axial stretching. At intermediate values, the competition between surface tension and stretching leads to a thickness that initially increases before decreasing near the exit.

5. The temperature-dependent problem

5.1. *Governing equations*

Now we show how the model derived above may be extended to describe non-isothermal tube drawing. Temperature variations are extremely important in practice because of their strong influence on the glass viscosity. Table 2 illustrates typical parameter values for this problem. The specific emissivity, ε_r, is a material constant that depends on the emissivity of the fluid as well as the geometry and surroundings of the experimental set-up (see, for example, Fitt et al. 2002; Šarboh, Milinković & Debeljković 1998). In reality, c_p, k_c, ε_r, α and the surface tension, γ, all vary with temperature. In practice, however, though the viscosity of the glass may vary by orders of magnitude over a relatively modest temperature range, these parameters

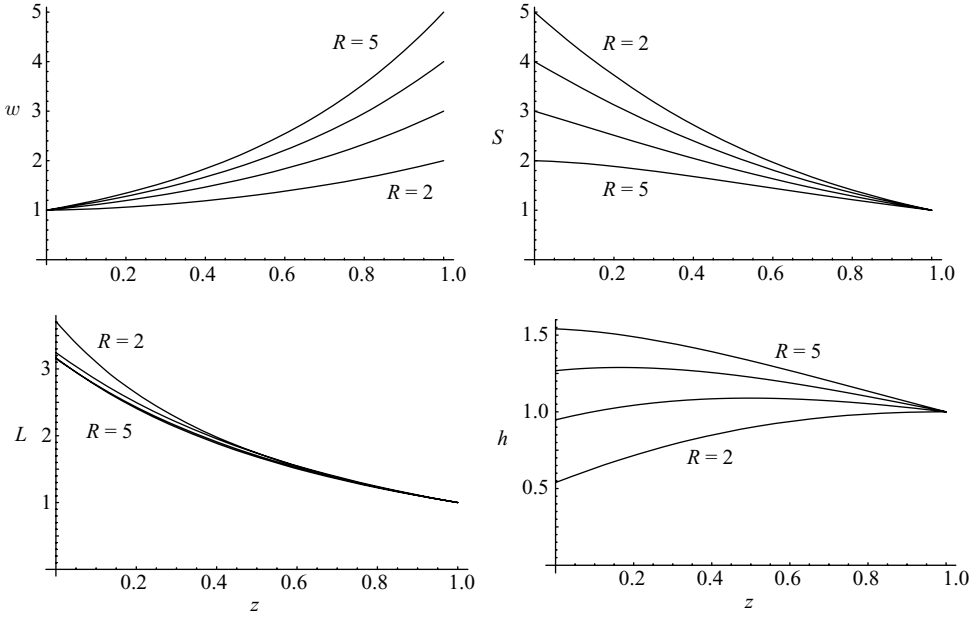

FIGURE 8. Axial velocity w, cross-section area S, tube circumference L and thickness h versus axial position z with $\gamma^* = 2$ and $R = 2, 3, 4, 5$.

Parameter	Symbol	Approx. value	Units
Input temperature[1]	T_0	1300	K
Specific heat[2]	c_p	770	$\mathrm{J\,kg^{-1}\,K^{-1}}$
Thermal conductivity[3]	k_c	1.1	$\mathrm{W\,m^{-1}\,K^{-1}}$
Stefan–Boltzmann constant[2]	σ	5.67×10^{-8}	$\mathrm{W\,m^2\,K^{-4}}$
Specific emissivity[2]	ε_r	0.9	—
Ambient temperature[1]	T_{am}	400	K
Input viscosity[1]	μ_0	2×10^3	Pa s
Temperature-viscosity parameter[4]	α	23	—

TABLE 2. Typical thermal parameter values for the drawing of capillary glass tubing. 1) U. Lange, personal communication (2006), 2) Šarboh *et al.* (1998), 3) Huang *et al.* (2003), 4) National Institute of Standards & Technology (1991).

are only weak functions of temperature (see, for example, Lee & Jaluria 1997). We therefore assume that these parameters are constant.

The fluid temperature is determined by conservation of energy via a control volume approach, accounting for diffusive and convective heat transfer, as well as radiative heat transfer to and from the surroundings, while neglecting viscous dissipation. The tubing is assumed to be sufficiently thin for the leading-order temperature T to be uniform over the cross-section, that is, we assume that the Biot number, $Bi = ch_d/k_c$, where c is the heat transfer coefficient, is small. Then $T(z)$ satisfies the dimensional equation (Huang *et al.* 2003, 2007)

$$\rho c_p w S \frac{\mathrm{d}T}{\mathrm{d}z} = \frac{\mathrm{d}}{\mathrm{d}z}\left(k_c S \frac{\mathrm{d}T}{\mathrm{d}z}\right) - \sigma \varepsilon_r L \left(T^4 - T_{\mathrm{am}}^4\right), \tag{5.1}$$

where the respective terms represent axial thermal convection, diffusion and radiative heating to and from the surroundings.

When we non-dimensionalize the temperature T with its value T_0 as it exits the die, the dimensionless version of (5.1) is

$$wS\frac{\mathrm{d}T}{\mathrm{d}z} = \frac{1}{Pe}\frac{\mathrm{d}}{\mathrm{d}z}\left(S\frac{\mathrm{d}T}{\mathrm{d}z}\right) - CL\left(T^4 - T_a^4\right), \tag{5.2}$$

where

$$Pe = \frac{\rho c_p w_0 D}{k_c} \tag{5.3}$$

is the Péclet number, and the other two dimensionless parameters are

$$C = \frac{\sigma \varepsilon_r T_0^3}{\epsilon \rho c_p w_0}, \quad T_a = \frac{T_{\mathrm{am}}}{T_0}. \tag{5.4}$$

The relationship between the viscosity and temperature of the glass depends largely on the specific chemical composition (see, for example, Karapet'yants 1960). In this paper we limit our attention to the simple exponential relation

$$\mu = \mu_0 \mathrm{e}^{\alpha(1-T/T_0)}, \tag{5.5}$$

where μ_0 is the viscosity at temperature T_0. The dimensionless parameter α is typically large, reflecting the extreme sensitivity of μ to variations in T. The physical applicability of relation (5.5) is considered in Karapet'yants (1960), and it is used in many mathematical models of tube drawing, for example Šarboh *et al.* (1998). The dimensionless version of (5.5) is

$$\mu = \mathrm{e}^{\alpha(1-T)}, \tag{5.6}$$

where μ is non-dimensionalized with its initial value μ_0.

Since T is uniform over each cross-section, it follows that μ is likewise a function only of z. It is then straightforward to generalize the axial flow equations (3.6) and (3.7) to

$$\frac{\mathrm{d}}{\mathrm{d}z}(wS) = 0, \tag{5.7}$$

$$ReSw\frac{\mathrm{d}w}{\mathrm{d}z} = \frac{\mathrm{d}}{\mathrm{d}z}\left(3\mu S\frac{\mathrm{d}w}{\mathrm{d}z}\right) + \gamma^*\frac{\mathrm{d}L}{\mathrm{d}z}, \tag{5.8}$$

with Re and γ^* now defined in terms of μ_0 rather than μ.

Because μ is constant in each cross-section, it is again possible to transform the crossflow problem into a standard two-dimensional Stokes flow problem, now defining the reduced Lagrangian time variable τ by

$$w\frac{\mathrm{d}\tau}{\mathrm{d}z} = \frac{\gamma^*}{\mu\sqrt{S}}, \quad \tau(1) = 0. \tag{5.9}$$

Otherwise, the transformation given in § 3.3 may be followed exactly, resulting in the equation

$$w\frac{\mathrm{d}}{\mathrm{d}z}\left(\frac{S}{L^2}\right) = \frac{\gamma^*}{\mu L}. \tag{5.10}$$

5.2. *Leading-order equations*

The parameter values in tables 1 and 2 suggest that $Pe \sim 10^3$, $\gamma^* \sim 10^2$ and C is order one, while T_a^4 is inevitably small, so we will neglect axial thermal diffusion and

radiative heating from the surroundings. We note that relatively small variations in input temperature produce dramatic changes in input viscosity and hence the value of γ^*. The parameter α is moderately large, but will be treated as order one for the moment. We also take the limit $Re \to 0$ as in § 4.

The boundary conditions are

$$w(0) = 1, \quad w(1) = R, \quad S(1) = 1, \quad L(1) = 1, \quad T(0) = 1. \tag{5.11a–e}$$

With $\mu(z)$ given by (5.6), a similar procedure to § 4.1 yields the analogous equations to (4.4) and (4.5),

$$\frac{\mathrm{d}w}{\mathrm{d}z} = \frac{(6bR - \gamma^* L)\, w \mathrm{e}^{\alpha(T-1)}}{3R}, \tag{5.12}$$

$$\frac{\mathrm{d}L}{\mathrm{d}z} = -\frac{(3bR + \gamma^* L)\, L \mathrm{e}^{\alpha(T-1)}}{3R}, \tag{5.13}$$

while, with $Pe \to \infty$ and $T_a \to 0$, (5.2) simplifies to

$$R\frac{\mathrm{d}T}{\mathrm{d}z} = -CLT^4. \tag{5.14}$$

The tube thickness h and cross-sectional area S may be recovered from the relations

$$h = \frac{R}{wL}, \qquad S = \frac{R}{w}, \tag{5.15}$$

while the evolution in the cross-section shape is determined by

$$\tau = 2\left(\frac{\sqrt{R}}{L\sqrt{w}} - 1\right). \tag{5.16}$$

5.3. *Solution*

By dividing (5.12) and (5.13), we obtain the first integral

$$w = \frac{R\,(3bR + \gamma^* L)^3}{L^2\,(3bR + \gamma^*)^3}, \tag{5.17}$$

which allows us to eliminate w from the problem. From the initial condition (5.11a), we obtain an equation for the dimensionless tension b in terms of the initial circumference $L_0 = L(0)$:

$$b = \frac{\gamma^*\left(L_0 R^{1/3} - L_0^{2/3}\right)}{3R\left(L_0^{2/3} - R^{1/3}\right)}. \tag{5.18}$$

It remains only to solve for L and T, subject to the boundary conditions

$$L(0) = L_0, \qquad T(0) = 1, \qquad L(1) = 1. \tag{5.19a–c}$$

With b given by (5.18), we can solve (5.13) and (5.14) as an initial-value problem, starting from $z = 0$ and using L_0 as a shooting parameter to satisfy the final condition (5.19c).

Further analytical progress may be made by dividing (5.13) and (5.14) to solve for L in terms of T in the form

$$L = \frac{L_0^{2/3}}{L_0^{2/3} - R^{1/3}}\left\{(L_0 - 1)\,\mathrm{e}^{-\gamma^* F_\alpha(T)/3C} - \left(L_0^{1/3} R^{1/3} - 1\right)\right\}. \tag{5.20}$$

The function $F_\alpha(T)$ is defined by

$$F_\alpha(T) = \int_T^1 \frac{\mathrm{e}^{\alpha(t-1)}}{t^4}\,\mathrm{d}t = \frac{1}{6}\left\{\alpha^3\mathrm{e}^{-\alpha}(Ei(\alpha) - Ei(\alpha T)) + \frac{\mathrm{e}^{\alpha(T-1)}}{T^3}(2+\alpha T+\alpha^2T^2) - (2+\alpha+\alpha^2)\right\}, \quad (5.21)$$

where Ei denotes the exponential integral

$$Ei(\alpha) = -\!\!\!\!\!\!\int_{-\alpha}^{\infty} \frac{\mathrm{e}^{-t}}{t}\,\mathrm{d}t. \quad (5.22)$$

The condition (5.19*c*) leads to a relation between L_0 and the final temperature $T_1 = T(1)$, namely

$$L_0 = \sqrt{R}\exp\left(\frac{\gamma^* F_\alpha(T_1)}{2C}\right). \quad (5.23)$$

Next we solve (5.14) for $T(z)$ in the implicit form

$$\frac{Cz}{R} = \left(1 - \frac{R^{1/3}}{L_0^{2/3}}\right)\int_T^1 \frac{t^{-4}\,\mathrm{d}t}{(L_0-1)\,\mathrm{e}^{-\gamma^* F_\alpha(t)/3C} - (L_0^{1/3}R^{1/3}-1)}, \quad (5.24)$$

and putting $z = 1$ we obtain the transcendental equation

$$\frac{C}{R}\left(1 - \mathrm{e}^{-\gamma^* F_\alpha(T_1)/3C}\right)^{-1} = \int_{T_1}^1 \frac{t^{-4}\,\mathrm{d}t}{(\mathrm{e}^{\gamma^* F_\alpha(T_1)/2C}\sqrt{R}-1)\mathrm{e}^{-\gamma^* F_\alpha(t)/3C} - (\mathrm{e}^{\gamma^* F_\alpha(T_1)/6C}\sqrt{R}-1)}. \quad (5.25)$$

The problem is solved completely once we have determined T_1 from (5.25). Equations (5.24) and (5.20) determine $T(z)$ and $L(z)$ parametrically, and we can then obtain $h(z)$ and $S(z)$ from (5.15) and $\tau(z)$ from (5.16), which may be rearranged to

$$1 + \frac{\tau}{2} = \frac{\sqrt{R}}{L\sqrt{w}} = \left(\frac{3bR+\gamma^*}{3bR+\gamma^* L}\right)^{3/2} = \exp\left(\frac{\gamma^*}{2C}(F_\alpha(T) - F_\alpha(T_1))\right). \quad (5.26)$$

5.4. *Parametric analysis*

Now the solution depends on two more dimensionless parameters α and C in addition to γ^* and R, and the task of mapping out parameter-space is therefore somewhat more onerous. The general structure is similar to that encountered in §4. For fixed values of α, C and γ^*, there is a minimum value of R below which (5.25) has no solution and above which there are two possible solutions for T_1. This behaviour is illustrated in figure 9(*a*), where we plot the dimensionless tension b, determined from (5.18) and (5.23) after solving (5.25) for T_1, versus the draw ratio R. Here we fix $\gamma^* = 2$, $\alpha = 1$ and various values of C between 0 and 1, and we only plot practically relevant values of $R > 1$. When $C = 0$, $T \equiv 1$ and we obtain the isothermal solution from §4. As C increases, the upper branch of solutions diverges rapidly from the $C = 0$ curve, while the close-up in figure 9(*b*) shows that the tension on the lower branch increases more gradually with increasing C. This is unsurprising, since C controls the rate at which the tube radiates heat: as the glass cools, its viscosity grows rapidly and the tension needed to achieve a given draw ratio thus increases. As argued in §4.2, we expect only the lower branch to be stable.

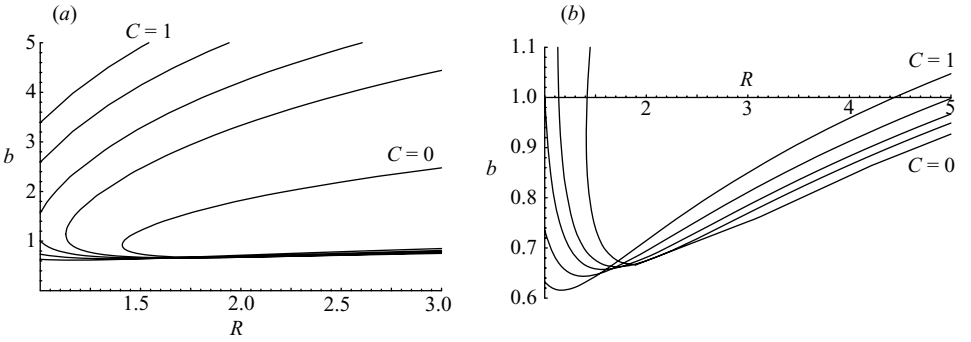

FIGURE 9. (*a*) Scaled tension b versus draw ratio R with surface tension parameter $\gamma^* = 2$, temperature-viscosity parameter $\alpha = 1$ and radiation parameter $C = 0, 0.125, 0.25, 0.5, 1.0$. (*b*) Close-up of the lower branch.

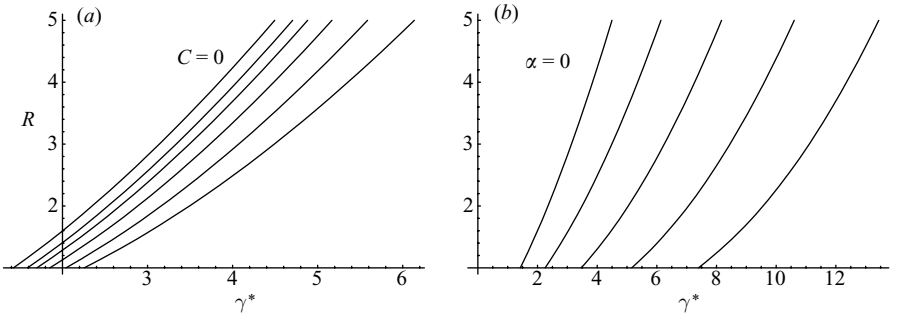

FIGURE 10. Curve in the (γ^*, R)-plane on which $\tau(0) = \tau_c \approx -1.46572$. (*a*) $\alpha = 1$ and $C = 0, 0.125, 0.25, 0.5, 1, 2$. (*b*) $C = 2$ and $\alpha = 0, 1, 2, 3, 4$.

Now, to identify the region of parameter-space where a viable tube can be formed, the easiest condition to impose is a limitation on $\tau(0)$ for the tube not to pinch off. If we define

$$\lambda = -\ln(1 + \tau(0)/2), \tag{5.27}$$

where $\tau(0)$ is held fixed, then

$$\gamma^* = \frac{2\lambda C}{F_\alpha(T_1)}, \tag{5.28}$$

and T_1 is determined as a function of λ, R, α and C by the transcendental equation

$$\frac{C}{R} = (1 - \mathrm{e}^{-2\lambda/3}) \int_{T_1}^{1} \frac{t^{-4}\,\mathrm{d}t}{\left(\mathrm{e}^{\lambda}\sqrt{R} - 1\right)\mathrm{e}^{-2\lambda F_\alpha(t)/3F_\alpha(T_1)} - \left(\mathrm{e}^{\lambda/3}\sqrt{R} - 1\right)}. \tag{5.29}$$

We display the results of this approach in figure 10, where we plot the curve in the (γ^*, R)-plane on which $\tau(0) = \tau_c \approx -1.46572$, the critical time at which our illustrative example in figure 3 pinches off; thus $\tau(0) > \tau_c \approx -1.46572$ only if R lies above this curve. In figure 10(*a*) we hold $\alpha = 1$ and vary C through the values used previously in figure 9. As we increase C, the viable region of parameter-space grows. Again this is due to the increase in viscosity, reducing the effect of surface tension which drives the evolution in the cross-section shape.

A similar effect is observed in figure 10(*b*), where we set $C = 1$ and vary α. When $\alpha = 0$, although the temperature is not constant, the viscosity does not vary with T

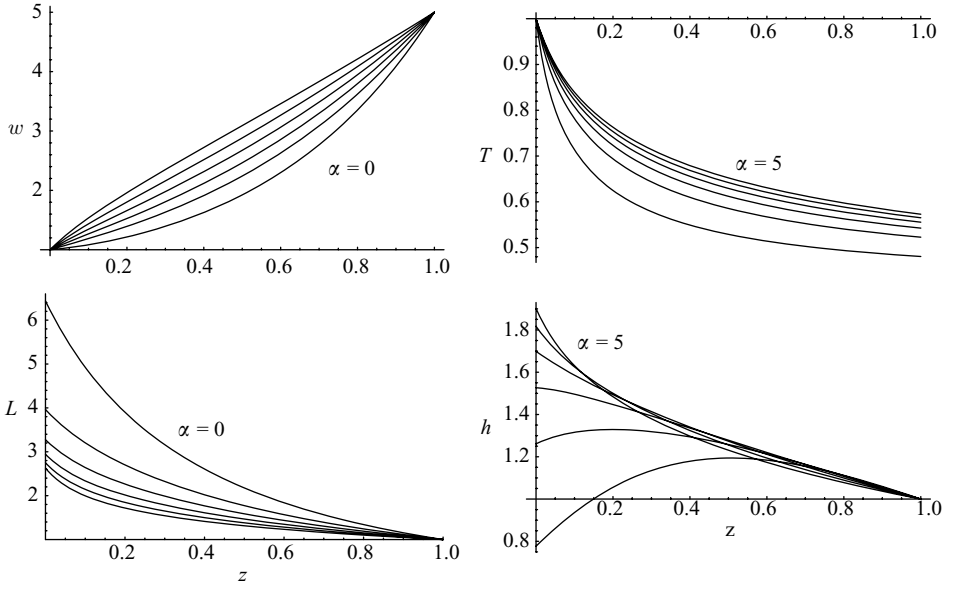

FIGURE 11. Axial velocity w, temperature T, tube circumference L and thickness h versus axial position z with $\gamma^* = 4$, $R = 5$, $C = 5$ and $\alpha = 0, 1, 2, 3, 4, 5$.

so the mechanical behaviour of the tube is identical to the isothermal solution. As α increases, the viscosity increases and the cross-section shape thus evolves more slowly, which again makes the tube less likely to pinch off.

5.5. *Typical solutions*

In figure 11, we show typical solutions for w, T, L and h with $\gamma^* = 4$, $R = 5$, $C = 5$ and $\alpha = 0, 1, 2, 3, 4, 5$. When $\alpha = 0$, the velocity, given by (4.6), grows roughly exponentially with z. As α increases, the viscosity becomes an increasing function of z. This penalizes stretching towards the downstream end of the tube and makes the variations in w closer to linear. This effect is also evident in the behaviour of L. As α increases, the variations in L are localized near $z = 0$ where the viscosity is relatively low. When $\alpha = 0$, the tube thickness h initially increases under surface tension before decreasing near the exit, but, for larger values of α, viscous effects dominate so h decreases throughout the tube.

In figure 12, we show the analogous solutions for larger, more realistic, values of α. As α increases, w, L and h become virtually constant outside a boundary layer near the die. Meanwhile, the temperature approaches

$$T(z) \sim \left(1 + \frac{3Cz}{R}\right)^{-1/3} \tag{5.30}$$

which is obtained from (5.14) with $L \sim 1$ and shown as a dashed line in figure 12.

5.6. *Asymptotic analysis*

In this section we exploit the largeness of the material parameter α for glass. This asymptotic limit is also examined for the stretching of heated threads in Howell *et al.* (2007). From (5.13), we deduce that $\mathrm{d}L/\mathrm{d}z$ is exponentially small when $T < 1$. This confirms the results seen in figure 12 that $L \sim 1$ and T is given to leading order by

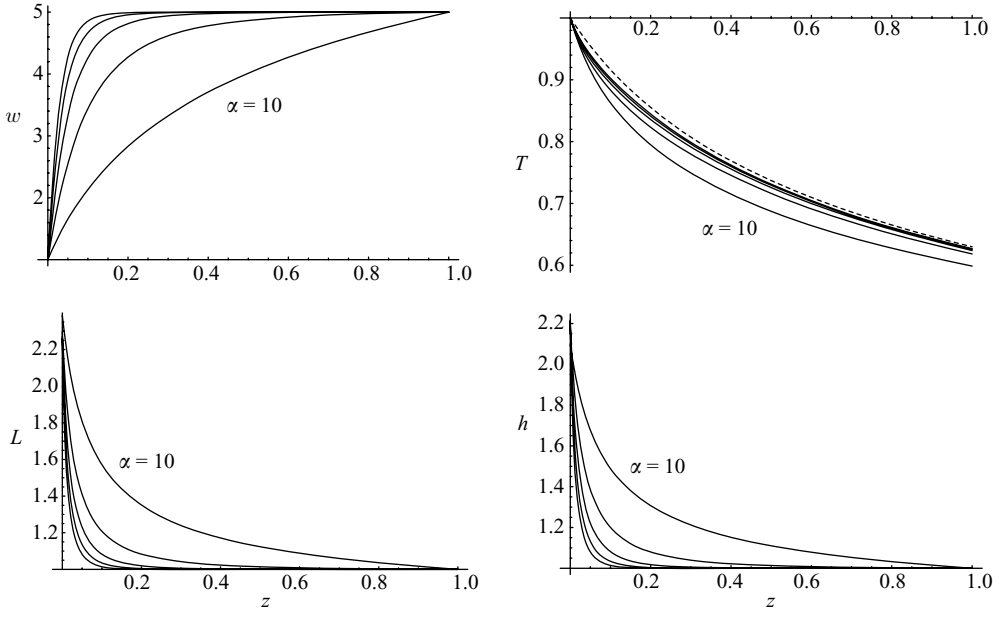

FIGURE 12. Axial velocity w, temperature T, tube circumference L and thickness h versus axial position z with $\gamma^* = 4$, $R = 5$, $C = 5$ and $\alpha = 10, 20, 30, 40, 50$.

(5.30). These approximations fail in a boundary layer near $z = 0$, where

$$z = \left(\frac{R}{\alpha C}\right) Z, \quad T = 1 - \frac{\phi}{\alpha}. \tag{5.31}$$

To obtain a sensible balance, we also require b to be asymptotically large, and a distinguished limit occurs when we rescale as follows:

$$b = \left(\frac{\alpha C}{R}\right) B, \quad \gamma^* = (3\alpha C)\,\varsigma. \tag{5.32}$$

The interpretation of these is that an enhanced viscosity leads to a higher tension and requires a higher value of γ^* for surface tension to have a significant influence. This is consistent with the observation that γ^* may be large in practice.

Following the scalings (5.32), equations (5.13) and (5.14) become

$$\frac{\mathrm{d}L}{\mathrm{d}Z} = -(B + \varsigma L) L \mathrm{e}^{-\phi}, \qquad \frac{\mathrm{d}\phi}{\mathrm{d}Z} = L, \tag{5.33}$$

to leading order in $1/\alpha$, with the initial conditions

$$L(0) = L_0, \qquad \phi(0) = 0. \tag{5.34}$$

By dividing the two equations (5.33), we find the first integral

$$\phi = -\ln\left\{1 - \frac{1}{\varsigma}\ln\left(\frac{B + \varsigma L_0}{B + \varsigma L}\right)\right\}, \tag{5.35}$$

and $L(Z)$ therefore satisfies

$$\frac{\mathrm{d}L}{\mathrm{d}Z} = -L\,(B + \varsigma L)\left\{1 - \frac{1}{\varsigma}\ln\left(\frac{B + \varsigma L_0}{B + \varsigma L}\right)\right\}. \tag{5.36}$$

From the matching condition $L \to 1$ as $Z \to \infty$, we deduce that

$$\frac{B + \varsigma L_0}{B + \varsigma} = \mathrm{e}^{\varsigma}, \tag{5.37}$$

and the exact equation (5.18) for b leads to a relation for the initial circumference, namely

$$\frac{L_0}{\sqrt{R}} = \mathrm{e}^{3\varsigma/2} = \mathrm{e}^{\gamma^*/2\alpha C}. \tag{5.38}$$

As $\alpha \to \infty$, with γ^* and C held fixed, we deduce that $L_0 \to \sqrt{R}$, and, indeed, we observe in figure 12 that $L(0)$ approaches $\sqrt{5} \approx 2.236$ as α increases.

This asymptotic analysis has the important result of predicting the size of the region over which geometrical variations in the tube will occur, namely $z = O(R/\alpha C)$. If this is too small, specifically if

$$\frac{R}{\alpha C} = O(\delta), \tag{5.39}$$

then our assumption of slow variation in the axial direction will fail. We note that very rapid necking of the tube near the die may be undesirable in practice, since it would lead to extreme sensitivity of the solution to the experimental conditions. The regions of parameter-space where our asymptotic theory breaks down should therefore probably be avoided anyway.

We also note that the boundary-layer thickness increases with increasing draw ratio, so the result (5.38) will break down when R is sufficiently large. Since the draw ratio is typically large in practice, it is worthwhile to explore further this distinguished asymptotic limit, in which the boundary layer fills the entire tube and $T \sim 1$ to leading order everywhere. We note from (5.38) that $L_0 = O(\sqrt{R})$ as $R \to \infty$ and therefore rescale

$$L = \sqrt{R}\ell, \qquad L_0 = \sqrt{R}\ell_0, \tag{5.40}$$

so that (5.18) becomes

$$b = \left(\frac{\alpha C \varsigma}{\sqrt{R}}\right) \frac{\ell_0}{\ell_0^{2/3} - 1} \tag{5.41}$$

to leading order in $1/R$, and hence (5.36) reduces to

$$\frac{\mathrm{d}\ell}{\mathrm{d}z} = -\left(\frac{\alpha C}{\sqrt{R}}\right) \ell \left(\ell + \frac{\ell_0}{\ell_0^{2/3} - 1}\right) \left\{\varsigma + \ln\left(\frac{(\ell_0^{2/3} - 1)\ell + \ell_0}{\ell_0^{5/3}}\right)\right\}. \tag{5.42}$$

The boundary conditions

$$\ell(0) = 1, \qquad \ell(1) = R^{-1/2}, \tag{5.43}$$

thus lead to the equation

$$\frac{\alpha C}{\sqrt{R}} = \int_{R^{-1/2}}^{1} \frac{\mathrm{d}\ell}{\ell \left(\ell + \dfrac{\ell_0}{\ell_0^{2/3} - 1}\right) \left\{\varsigma + \ln\left(\dfrac{(\ell_0^{2/3} - 1)\ell + \ell_0}{\ell_0^{5/3}}\right)\right\}}, \tag{5.44}$$

for ℓ_0.

The integral on the right-hand side diverges as $R \to \infty$, and the rate at which it does so depends on the relation between ℓ_0 and ς. We can recover the boundary-layer

solution found above by writing

$$\ell_0 \sim \mathrm{e}^{3\varsigma/2} + \frac{\ell_0^{(1)}}{\sqrt{R}} + \cdots, \tag{5.45}$$

in which case (5.44) becomes an equation for $\ell_0^{(1)}$, namely

$$\frac{\alpha C}{R} = -\frac{3\,(\mathrm{e}^{\varsigma} - 1)}{2\ell_0^{(1)}} \ln\left(1 - \frac{2\ell_0^{(1)}}{3\,(\mathrm{e}^{\varsigma} - 1)}\right). \tag{5.46}$$

This verifies that (5.44) is consistent with (5.38) when $\alpha C/R$ is order one.

Otherwise, ℓ_0 is not asymptotically close to $\mathrm{e}^{3\varsigma/2}$ and the integral in (5.44) has only a logarithmic singularity as $R \to \infty$. To investigate the behaviour more closely, we subtract off the singular part of the integrand and introduce the shorthand

$$\varrho = \varsigma - \frac{2}{3}\ln \ell_0 = \frac{\gamma^*}{3\alpha C} - \frac{1}{3}\ln\left(\frac{L_0^2}{R}\right), \tag{5.47a}$$

$$\Lambda = \frac{\ell_0^{2/3} - 1}{\ell_0} = \frac{R^{1/6}\big(L_0^{2/3} - R^{1/3}\big)}{L_0}, \tag{5.47b}$$

to write (5.44) in the form

$$\frac{\alpha C}{\sqrt{R}\ln R} = \frac{\Lambda}{2\varrho}\left\{1 - \frac{2}{\ln R}\int_0^{\Lambda} \frac{\varrho\xi + (1+\xi)\ln(1+\xi)}{\xi(1+\xi)(\varrho + \ln(1+\xi))}\,\mathrm{d}\xi\right\}, \tag{5.48}$$

after neglecting terms of order $R^{-1/2}$.

We infer that the distinguished limit in which all effects balance along the entire tube occurs when both ς and the parameter $\alpha C/\sqrt{R}\ln R$ are order one. If we are content to discard the logarithmically small term in (5.48), we find that ℓ_0 satisfies the equation

$$\frac{\alpha C}{\sqrt{R}\ln R} = \frac{3\big(\ell_0^{2/3} - 1\big)}{2\ell_0\,(3\varsigma - 2\ln \ell_0)}. \tag{5.49}$$

We note that the right-hand side of (5.49) is a non-monotonic function of ℓ_0 when $\varsigma > 2\ln 3 + 8/3 \approx 4.864$, which once again raises the possibility of non-uniqueness. However, we do not bother to analyse the relation (5.49) further, since we do not expect it to give a reliable approximation to (5.48) at realistic values of R.

In figure 13, we illustrate the asymptotic structure revealed in this section by plotting the circumference L versus z with $C = 1$ and increasing values of α, while γ^* and R are varied to keep $\varsigma = 1/2$ and $\alpha C/\sqrt{R}\ln R = 3$. Even for large values of α, variations in L occur throughout the tube, rather than just in a boundary layer like those seen in figure 12. Furthermore, when we plot $\ell = L/\sqrt{R}$ rather than L, the graphs appear to converge near $z = 0$ as α increases (although they must differ as $z \to 1$, where $L \to 1$).

In figure 14 we show the three-dimensional tube profile and cross-sections through the tube corresponding to the largest value of α in figure 13, that is with $\alpha = 50$, $C = 1$, $R = 26.104$ and $\gamma^* = 75$. As we have seen earlier, these values are by no means unrealistic in practice. Again we observe that variations in L and h occur all along the tube, but it is clear that the tube geometry evolves significantly more rapidly near the top, where the glass is hotter. In particular, the cross-sectional shape is already very close to its final square configuration at $z = 1/4$.

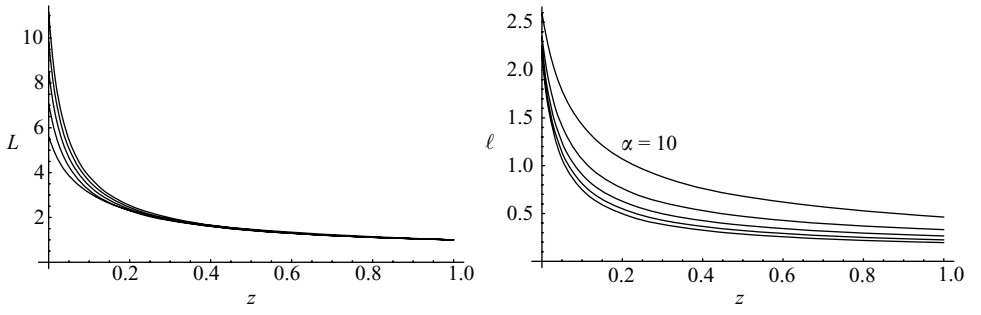

FIGURE 13. Tube circumference L and scaled circumference $\ell = L/\sqrt{R}$ versus axial position z with $C = 1$, $\gamma^* = 3\alpha/2$ and $\alpha = 10$, $R = 4.673$; $\alpha = 20$, $R = 9.107$; $\alpha = 30$, $R = 14.203$; $\alpha = 40$, $R = 19.886$; $\alpha = 50$, $R = 26.104$.

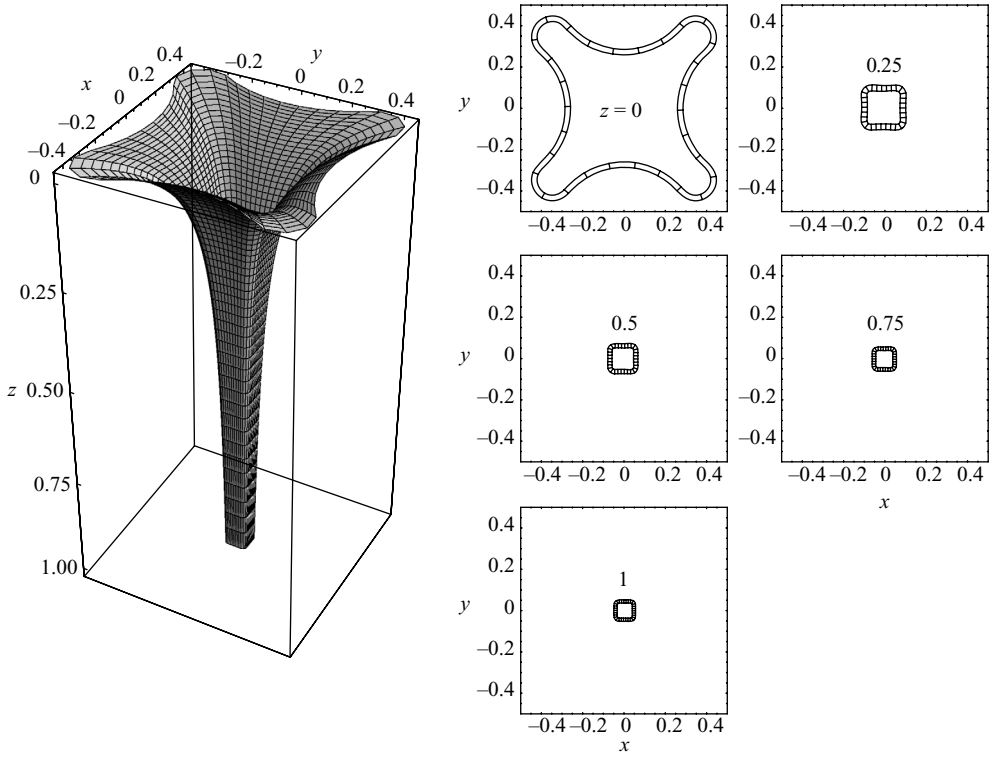

FIGURE 14. Three-dimensional centreline profile with $\gamma^* = 75$, $R = 26.104$, $\alpha = 50$, $C = 1$ and $k = 20$, as well as cross-sections through the tube with $\epsilon = 0.05$.

The conclusion of our asymptotic analysis is that, when α and R are large, the behaviour of the solution is governed by two key parameters, namely $\alpha C/\sqrt{R}\ln R$ and $\gamma^*/C\alpha$. When $\alpha C/\sqrt{R}\ln R$ is large, geometrical variations in the tube take place in a boundary layer near $z = 0$; if it is small, then thermal effects have a negligible influence on the shape of the tube. On the other hand, the importance of surface tension is measured by $\gamma^*/C\alpha$. If this parameter is small, then surface tension is negligible, and the cross-section shape is approximately conserved along the tube. If it is large, then dramatic changes in cross-section shape will occur along the tube,

and pinch-off at $z = 0$ will be increasingly likely, thus eliminating the existence of a physically realizable die shape.

6. Conclusions

This paper concerns the steady drawing of a slowly varying three-dimensional non-axisymmetric tube, evolving under the action of surface tension. The assumption of slow variations in the axial direction allowed us to use a quasi-one-dimensional model, in which the tube is characterized by its cross-section area S and centreline circumference L, and the axial velocity w, all of which are functions only of z. In addition, we exploited the result that each material cross-section evolves as a two-dimensional unsteady Stokes flow when expressed in suitable scaled Lagrangian coordinates. By assuming that the tube walls are thin, we were thus able to determine the evolution of the circumference and shape of the cross-section using the model for a two-dimensional annular viscous tube derived previously by Griffiths & Howell (2007). We thus solved an inverse problem, in which the final shape of the tube is specified, and the die shape required to produce it is found as part of the solution.

For isothermal tube drawing, with negligible inertia, we found that the problem can be solved explicitly, with just one parameter b, representing the dimensionless tension in the tube, remaining to be determined from a transcendental equation. We discovered that, depending on the draw ratio and the surface tension coefficient, there may be two or no solutions for b, and we mapped out the regions of the (γ^*, R) parameter-space where stable, viable solutions are likely to exist. In our sample solutions, the most striking result is the variation in the tube thickness h, which evolves under a competition between surface tension and axial stretching. When these effects are in balance, h behaves non-monotonically, first increasing as the tube exits the die before decreasing again near the exit.

We then extended the model to include temperature variations, which are coupled to the mechanical behaviour of the tube via the strongly temperature-dependent viscosity. Again, the problem admits analytic solution, albeit in an awkward implicit form, and is fully determined by the solution of a single transcendental equation. Now there are four dimensionless parameters to consider, but the structure of parameter-space is qualitatively similar to that encountered in the isothermal limit. As the surface tension increases, an increasing draw ratio is required to prevent the tube from pinching off. Increasing either the radiative cooling or the sensitivity of the viscosity to temperature variations has the effect of increasing the viscosity along the tube and thus delays the occurrence of pinch-off.

In practice, the viscosity of glass can vary by many orders of magnitude over the temperature ranges of interest, and the sensitivity parameter α is therefore typically large. We found that, as α increases, the geometrical variations in the tube become localized in a small boundary layer near the die. This effect is counteracted by also increasing the draw ratio, and we found that $\alpha C/\sqrt{R}\ln R$ is the critical parameter controlling the length of the boundary layer. Our analysis also revealed that $\gamma^*/\alpha C$ determines the influence of surface tension on the tube shape.

If the tube cross-section does indeed evolve very rapidly, then our slowly varying assumption is called into question. In such cases, there will be a region near the die in which the tube is fully three-dimensional, although still thin. The behaviour in this region may be described using the 'viscous shell' theory of Pearson & Petrie (1970*a*,*b*) and Howell (1996), and then matched with our slowly varying model. We note, however, that quasi-one-dimensional models of fibre drawing have historically

proved extremely successful, often giving remarkably accurate results even outside their formal limits of applicability.

In this paper, we have only considered steady tube drawing, although it is straightforward to generalize our equations to include time variations. Since we have encountered both non-existence and non-uniqueness of solutions, it would be worthwhile exploring their linear stability. We have found generically that the draw ratio R must exceed some critical lower bound for a physically sensible solution to exist. However, it is well-known that an excessive draw ratio may lead to the so-called 'draw resonance' instability (Pearson & Matovich 1969), and this may impose further restrictions on the parameter values for which a tube can be successfully formed.

In refining our initial simple model, we concentrated on non-isothermal effects, which are likely to be particularly significant in practice due to the consequent large variations in viscosity. However, there are many further physical effects that could also be included. For example, it is easy to replace the viscosity-temperature relation (5.5) with some other empirical formula such as the Vogel–Fulcher–Tammann law (Krause & Loch 2002). We have found that such generalizations do not significantly alter the behaviour of the solutions presented in this paper.

We have not considered radiative heat transfer in the glass. This is a formidable problem in general, but is often simplified using the so-called Rosseland approximation, which leads to a nonlinear diffusion equation for the temperature T (see, for example Myers 1989; Paek & Runk 1978). This may well decrease the effective Péclet number and invalidate our conclusion that axial thermal diffusion is negligible.

Finally, we note that additional control over the tube may be achieved by pressurizing the hole, a technique used in axisymmetric tube drawing to help prevent closure of the hole (Fitt *et al.* 2001, 2002). Griffiths & Howell (2007) have shown how to incorporate an applied pressure in the two-dimensional crossflow equation (3.16), and it is straightforward in principle to apply their results to a slowly varying tube as demonstrated in this paper.

This research was supported by a studentship from the University of Oxford's EPSRC-funded doctoral training account. The authors gratefully acknowledge helpful discussions with Dr H. J. J. Gramberg, Professor E. J. Hinch, Professor J. R. Lister and Dr J. R. Ockendon. We were introduced to this problem by U. Lange from Schott AG, who gave us invaluable insight into the practical issues involved.

REFERENCES

Buckmaster, J. D. & Nachman, A. 1978 The buckling and stretching of a viscida II. Effects of surface tension. *Q. J. Mech. Appl. Maths* **31**, 157–168.

Buckmaster, J. D., Nachman, A. & Ting, L. 1975 The buckling and stretching of a viscida. *J. Fluid Mech.* **69**, 1–20.

Cummings, L. J. & Howell, P. D. 1999 On the evolution of non-axisymmetric viscous fibres with surface tension, inertia and gravity. *J. Fluid Mech.* **389**, 361–389.

Denn, M. 1980 *Process Fluid Mechanics*. Prentice Hall.

Dewynne, J. N., Ockendon, J. R. & Wilmott, P. 1989 On a mathematical model for fibre tapering. *SIAM J. Appl. Maths* **49**, 983–990.

Fitt, A. D., Furusawa, K., Monro, T. M. & Please, C. P. 2001 Modeling the fabrication of hollow fibres: Capillary drawing. *IEEE J. Lightwave Technol.* **19**, 1924–1931.

Fitt, A. D., Furusawa, K., Monro, T. M., Please, C. P. & Richardson, D. A. 2002 The mathematical modelling of capillary drawing for holey fibre manufacture. *J. Engng. Maths* **43**, 201–227.

Graham, S. J. 1987 Mathematical modelling of glass flow in container manufacture. PhD thesis, University of Sheffield.

Griffiths, I. M. 2008 Mathematical modelling of non-axisymmetric glass tube manufacture. PhD thesis, University of Oxford.

Griffiths, I. M. & Howell, P. D. 2007 The surface-tension-driven evolution of a two-dimensional annular viscous tube. *J. Fluid Mech.* **593**, 181–208.

Howell, P. D. 1996 Models for thin viscous sheets. *Eur. J. Appl. Maths* **7**, 321–343.

Howell, P. D., Wylie, J. J., Huang, H & Miura, R. M. 2007 Stretching of heated threads with temperature-dependent viscosity: asymptotic analysis. *Discrete Continuous Dyn. Syst.* **7**, 553–572.

Huang, H., Miura, R. M., Ireland, W. P. & Puil, E. 2003 Heat-induced stretching of a glass tube under tension: Application to glass microelectrodes. *SIAM J. Appl. Maths* **63**, 1499–1519.

Huang, H., Wylie, J. J., Miura, R. M. & Howell, P. D. 2007 On the formation of glass microelectrodes. *SIAM J. Appl. Maths* **67**, 630–666.

Karapet'yants, M. Kh. 1960 The viscosity-temperature relationship for silicate glasses. *Glass Ceramics* **15**, 26–32.

Krause, D. & Loch, H. 2002 *Mathematical Simulation in Glass Technology*. Springer.

Lee, S. H.-K. & Jaluria, Y. 1997 Simulation of the transport process in the neck-down region of a furnace drawn optical fibre. *Intl J. Heat Mass Transfer* **40**, 843–856.

Myers, M. R. 1989 A model for unsteady analysis of preform drawing. *AIChE J.* **35**, 592–601.

National Institute of Standards & Technology 1991 *Standard Reference Material 710a. Soda-Lime-Silica Glass*. http://glassproperties.com/standards.

Paek, U. C. & Runk, R. B. 1978 Physical behaviour of the neck-down region during furnace drawing of silica fibres. *J. Appl. Phys.* **49**, 4417–4422.

Papamichael, H. & Miaoulis, I. N. 1991 Thermal behavior of optical fibers during the cooling stage of the drawing process. *J. Mater. Res.* **6**, 159–167.

Pearson, J. R. A. & Matovich, M. A. 1969 Spinning a molten threadline. Stability. *Ind. Engng Chem. Fund.* **8**, 605–609.

Pearson, J. R. A. & Petrie, C. J. S. 1970*a* The flow of a tubular film. Part 1. Formal mathematical representation. *J. Fluid Mech.* **40**, 1–19.

Pearson, J. R. A. & Petrie, C. J. S. 1970*b* The flow of a tubular film. Part 2. Interpretation of the model and discussion of solutions. *J. Fluid Mech.* **42**, 609–625.

Pfaender, H. G. 1996 *Schott Guide to Glass*. Chapman and Hall, London.

Šarboh, S. D., Milinković, S. A. & Debeljković, D. L. J. 1998 Mathematical model of the glass capillary tube drawing process. *Glass Technol.* **39**, 53–67.

Sivko, A. P. 1976 The production of glass tubes using the Vello method. *Glass Ceramics* **33**, 728–730.

Uhlmann, D. R. & Kreidl, N. J. 1984 *Glass. Science and Technology. Volume 2. Processing I*. Academic.

Voyce, C. J., Fitt, A. D. & Monro, T. M. 2004 Mathematical model of the spinning of microstructured optical fibres. *Optics Express* **12**, 5810–5820.

Wu, C. Y., Somervell, A. R. D. & Barnes, T. H. 1998 Direct image transmission through a multi-mode square optical fiber. *Optics Commun.* **157**, 17–22.

Wu, C. Y., Somervell, A. R. D., Haskell, T. G. & Barnes, T. H. 2000 Optical sine transformation and image transmission by using square optical waveguide. *Optics Commun.* **175**, 27–32.

Wylie, J. J., Huang, H. & Miura, R. M. 2007 Thermal instability in drawing viscous threads. *J. Fluid Mech.* **570**, 1–16.